Quantum control of nuclear wave packets by locally designed optimal pulses

Y. Ohtsuki, H. Kono, and Y. Fujimura
Department of Chemistry, Graduate School of Science, Tohoku University, Aoba-ku, Sendai 980-8578, Japan

(Received 14 May 1998; accepted 25 August 1998)

A new approach to locally design a control pulse is proposed. This locally optimized control pulse is explicitly derived, starting with optimal control formalism, and satisfies the necessary condition for a solution to the optimal control problem. Our method requires a known function, $g(t)$, *a priori*, which gives one of the possible paths within the functional space of the objective functional. A special choice of $g(t) \equiv 0$ reduces the expression of the control pulse to that derived by Kosloff *et al.* For numerical application, we restrict ourselves to this special case; however, by combining an appropriate choice of the target operator together with the backward time-propagation technique, we apply the local control method to population inversion and to wave packet shaping. As an illustrative example, we adopt a two-electronic-surface model with displaced harmonic potentials and that with displaced Morse potentials. It is shown that our scheme successfully controls the wave packet dynamics and that it can be a convenient alternative to the optimal control method for wave packet shaping. © *1998 American Institute of Physics.* [S0021-9606(98)00645-X]

I. INTRODUCTION

Application of the optimal control theory to molecular systems offers a general and flexible approach for designing optimal pulses to control chemical dynamics.[1–4] This method leads to coupled nonlinear equations whose numerical implementation needs an intensive iteration procedure. Although several efficient algorithms have been developed,[5–9] this method is often computationally too expensive. Thus, from a practical viewpoint, approximate treatments that are computationally less expensive are required. Perturbation approximation is sometimes employed to linearize an expression of an optimal pulse, assuming a weak-field regime.[10–20]

Another treatment is called the local control method,[21–29] which was first proposed by Kosloff *et al.*[3] and has been extensively developed by Tannor and co-workers,[21–26] and others.[27–29] In this treatment, a target operator is introduced to specify an objective state of a molecule. As a simple example, let us consider the case where the target operator is chosen so that it has a maximum value when the molecule reaches the objective state. Then one requires that the time-derivative of the average value of the target operator should have a positive value at any time to guarantee a monotonic increase. From this physical intuition, Kosloff *et al.*[3] derived an expression of local control pulse. Although any approximated treatment must be related to the optimal control method as long as they have the common goal of optimal field design, the relation between optimal and local control pulses is not clear. In our previous paper,[29] we applied perturbation expansion to the optimal control pulse within small time intervals to connect the local control method with the optimal method.

In this paper, we develop a novel local control method based on the optimal control theory. Our scheme has a similarity to the tracking problem,[30–33] which is inverse quantum mechanical control. The local control pulse derived by Kosloff *et al.*[3] is reduced to a special case of our control pulse. In numerical applications, we restrict ourselves to this special case; however, we show that an appropriate choice of target operator and backward time propagation can make it possible to control wave packet dynamics. The importance of the choice of the target operator, which determines the structure of the functional space, is also discussed using few-level systems.

In Sec. II, a formal theory is developed. The relation between our local control method and the tracking problem is discussed here. In Sec. III, the local control method is applied to population inversion of two- and three-level systems to see its feedback mechanism. We also analyze how the structure of the objective functional changes the excitation processes. In Sec. IV, wave packet shaping by the local control method is demonstrated using a two-electronic-state model with displaced harmonic potentials and that with displaced Morse potentials.

II. THEORY

A. Locally designed optimal control pulse

According to the formulation of the optimal control method,[1–4] we first introduce a target operator, W, whereby an objective state of a molecule is specified. We assume that a function, F, of the average value of the target operator has a maximum value when the molecule reaches the objective state. In this treatment, the optimal pulse gives a maximum value to the functional $F[\langle W(t_f)\rangle]$ at a controlling time, t_f. Mathernatically, the optimal pulse leads to an extremal value of the objective functional $J[E(t)]$ defined by

$$J[E(t)]=F[\langle W(t_f)\rangle]-\int_{t_0}^{t_f}dt\,\frac{1}{\hbar A(t)}\,[E(t)]^2, \tag{2.1}$$

where the second term represents the penalty due to the laser energy. The positive function of time $A(t)$ is chosen to weight the significance of it. In Eq. (2.1), the constraint originating from the equation of motion is assumed to be included through a time-evolution operator, and therefore there are no Lagrange's multipliers associated with the equation of motion. This is the reason why J is a functional only of the electric fields.

We rewrite Eq. (2.1) as

$$J[E(t)]=\int_{t_0}^{t_f}dt\left\{\frac{d}{dt}\,F[\langle W(t)\rangle]-\frac{1}{\hbar A(t)}\,[E(t)]^2\right\}+F[\langle W(t_0)\rangle]. \tag{2.2}$$

Consider the special case where the integrand in Eq. (2.2) is given by

$$\frac{d}{dt}\,F[\langle W(t)\rangle]-\frac{1}{\hbar A(t)}\,[E(t)]^2=g(t), \tag{2.3}$$

where $g(t)$ is *a known function of time*. Here we would like to emphasize that this function $g(t)$ is a given function of time and is not allowed to vary, and that it *should not* be a functional of electric fields. Then the objective functional has a form of

$$J[E(t)]=\int_{t_0}^{t_f}dt\,g(t)+F[\langle W(t_0)\rangle]. \tag{2.4}$$

Since the molecular state is initially specified, all the terms that appear in the right-hand side of Eq. (2.4) are constants. This means that the pulse satisfying Eq. (2.3) leads to $\delta J=0$, and therefore such a pulse can be a candidate for the solution to the optimal control problem. Furthermore, the requirement that the pulse should satisfy Eq. (2.3) at any time makes the problem local. This is our basic idea for obtaining a locally designed optimal pulse. In the following, the control pulse obtained by solving Eq. (2.3) is called a local control pulse for simplicity. It is worth noting, however, that our local control pulse satisfies the necessary condition for the optimal control pulse.

In the present paper, we restrict ourselves to control problems without dissipation so that the molecular dynamics can be described by the Schrödinger equation. (The inclusion of relaxation is possible by straightforward extension based on density matrix formalism.) Consider a molecule interacting with a time-dependent electric field $E(t)$ through the electric dipole interaction. The Hamiltonian of this system is given by

$$H^t=H_0+V^t=H_0-\mu E(t), \tag{2.5}$$

where H_0 is a molecular Hamiltonian, V^t is an interaction Hamiltonian, and μ is a transition dipole moment operator. The molecular system obeys the time-dependent Schrödinger equation

$$i\hbar\,\frac{d}{dt}\,|\psi(t)\rangle=H^t|\psi(t)\rangle. \tag{2.6}$$

By differentiating $F[\langle W(t)\rangle]$ with respect to t in Eq. (2.3), we obtain the quadratic equation for the local control pulse,

$$[E(t)]^2-iA(t)\lambda(t)\langle\psi(t)|[W,\mu]|\psi(t)\rangle E(t)+iA(t)\lambda(t)\langle\psi(t)|[W,H_0]|\psi(t)\rangle+\hbar A(t)g(t)=0, \tag{2.7}$$

where

$$\lambda(t)=\left.\frac{dF(X)}{dX}\right|_{X=\langle W(t)\rangle}. \tag{2.8}$$

In deriving Eq. (2.7), explicit time-dependence of the target operator has been ignored. Since the electric field $E(t)$ is a real quantity, a positive discriminant for the quadratic equation of $E(t)$ is required at any time $t\in[t_0,t_f]$.

In the present paper, we will concentrate on the special case that always gives us a solution, rather than discuss the discriminant in detail. For this purpose, let us assume that the target operator commutes with the molecular Hamiltonian

$$[W,H_0]=0. \tag{2.9}$$

If the function $g(t)$ is chosen as

$$g(t)=0, \tag{2.10}$$

then Eq. (2.7) is reduced to

$$E(t)\{E(t)-iA(t)\lambda(t)\langle\psi(t)|[W,\mu]|\psi(t)\rangle\}=0. \tag{2.11}$$

The solution $E(t)=0$ is allowed only in the trivial case of starting out in the objective state. Thus, we obtain the expression for the local control pulse,

$$E(t)=-2A(t)\lambda(t)\mathrm{Im}\langle\psi(t)|W\mu|\psi(t)\rangle. \tag{2.12}$$

Due to the condition of Eq. (2.10), the value of the objective functional J is determined by the initial condition

$$J[E(t)]=F[\langle W(t_0)\rangle], \tag{2.13}$$

which may be one of the maximal values of the functional. From Eq. (2.3), however, the condition of $g(t)=0$ leads to

$$\frac{d}{dt}\,F[\langle W(t)\rangle]=\frac{1}{\hbar A(t)}\,[E(t)]^2>0. \tag{2.14}$$

This means that the value of $F[\langle W(t)\rangle]$ increases in proportion to the pulse energy. Since the objective state gives the maximum value to $F[\langle W(t)\rangle]$, the local control pulse always brings the molecule towards the objective state. The ''quality'' of the control pulse depends on the target operator W and the function F as well as on the weight $A(t)$. A better choice of these properties can result in the construction of a more suitable functional form of J in the sense that it can improve the achievement and give a better shape of the pulse.

B. Pulse shaping in the rotating wave-approximation

Next we derive the local control pulse under the rotating wave-approximation (RWA). Under the RWA, the interaction Hamiltonian is given by the resonant-interaction terms

$$V^t = -\mu_+ \epsilon(t) - \mu_- \epsilon^*(t), \tag{2.15}$$

where the transition moment operator μ_+ (μ_-) corresponds to the absorption (emission) process. In this case, we start with the objective functional

$$J[\epsilon(t), \epsilon^*(t)] = F[\langle W(t_f)\rangle] - \int_{t_0}^{t_f} dt \, \frac{2}{\hbar A(t)} |\epsilon(t)|^2, \tag{2.16}$$

where the penalty of the pulse energy only includes the rotating parts. Introducing *a known function* $g(t)$, we can derive the local control pulse in the same manner as shown in the previous section. If we assume the commutation relation of Eq. (2.9) and consider a special case of $g(t)=0$, then we have the following expression:

$$\epsilon(t) = iA(t)\lambda(t)\langle\psi(t)|[W, \mu_-]|\psi(t)\rangle. \tag{2.17}$$

This implies that under the RWA, we can calculate the control pulse in a rotating frame. To see this explicitly, we introduce a rotating frame that is characterized by a unitary operator,

$$R(t, t_0) = \exp[-iS(t-t_0)], \tag{2.18}$$

where the operator S shifts the molecular energy by $\hbar\omega_r$. Substituting the operator $R(t,t_0)$ into Eq. (2.17) and using the relation

$$R^\dagger(t,t_0)\mu_\pm R(t,t_0) = \exp[\pm i\omega_r(t-t_0)]\mu_\pm, \tag{2.19}$$

we can obtain

$$\epsilon(t) = \epsilon_r(t)\exp[-i\omega_r(t-t_0)] \tag{2.20a}$$

with

$$\epsilon_r(t) = iA(t)\lambda(t)\langle\psi_r(t)|[W, \mu_-]|\psi_r(t)\rangle. \tag{2.20b}$$

Here $|\psi_r(t)\rangle$ denotes the wave function on the rotating frame, which obeys the Schrödinger equation with the Hamiltonian

$$\begin{aligned} H_r^t &= (H_0 - \hbar S) + V_r^t \\ &= (H_0 - \hbar S) - \mu_+ \epsilon_r(t) - \mu_- \epsilon_r^*(t). \end{aligned} \tag{2.21}$$

This indicates that the control pulse can be calculated on the rotating frame and that the result $\epsilon_r(t)$ can be easily related to the original pulse by Eq. (2.20a). Since we can remove rapidly oscillating components from the Hamiltonian [Eq. (2.21)], an appropriate choice of ω_r can considerably improve computational efficiency.

C. Relation to other pulse-design schemes

Our method is closely related to those previously proposed and may be connected with several ideas. In our previous paper,[29] we derived Eq. (2.12) [in a special case of $\lambda(t)=1$ and $A(t)=A$] by applying perturbative expansion to an expression of the optimal control pulse. That is, we divide the whole time $[t_0, t_f]$ into N small time intervals,

$$t_k = t_0 + \frac{t_f - t_0}{N} k, \quad (k = 0,1,2,...,N), \tag{2.22}$$

and successively apply the optimal control method to these small time intervals. If the time-evolution operators are approximated by free propagators in each time step, then the control pulse at time $t \in [t_k, t_{k+1}]$ is expressed as

$$\begin{aligned} E(t) = -A(t)\lambda(t)\mathrm{Im}\langle\psi(t)|U_0^\dagger \\ \times(t_{k+1},t)WU_0(t_{k+1},t)\mu|\psi(t)\rangle, \end{aligned} \tag{2.23}$$

where the free propagator is defined by

$$U_0(t_{k+1}, t) = \exp[-iH_0(t_{k+1}-t)/\hbar]. \tag{2.24}$$

In this expression, there still remains a global nature in the sense that it explicitly includes the future time $t_{k+1}(>t)$. However, in the case where a target operator commutes with the zero-order molecular Hamiltonian H_0 [Eq. (2.9)], the expression of the optimal pulse is reduced to

$$E(t) = -A(t)\lambda(t)\mathrm{Im}\langle\psi(t)|W\mu|\psi(t)\rangle, \tag{2.25}$$

and we can therefore remove all future information. Except for the constant factor 2, this has the same form as that in Eq. (2.12). In the limit of $N\uparrow\infty$, the time interval $\Delta t\downarrow 0$ and the time-evolution of the system can be neglected because $U_0(\Delta t)\approx 1$. Then the system may be approximated by a time-invariant system.[28]

A local control scheme was first proposed and developed by Kosloff, Tannor, and co-workers.[3,21–26] For convenience, we will examine their idea using our notation introduced in Sec. II A. Let us consider the time-derivative of $F[\langle W(t)\rangle]$,

$$\begin{aligned} \frac{d}{dt}F[\langle W(t)\rangle] = \frac{i}{\hbar}\lambda(t)\langle\psi(t)|[H_0, W]|\psi(t)\rangle \\ - \frac{i}{\hbar}\lambda(t)\langle\psi(t)|[\mu, W]|\psi(t)\rangle E(t). \end{aligned} \tag{2.26}$$

If we assume that the target operator commutes with the molecular Hamiltonian H_0, then Eq. (2.26) becomes

$$\frac{d}{dt}F[\langle W(t)\rangle] = -\frac{2}{\hbar}\lambda(t)\mathrm{Im}\{\langle\psi(t)|W\mu|\psi(t)\rangle\}E(t). \tag{2.27}$$

Therefore, in order for the time derivative to have a positive value at any time, the electric field must have the form of

$$E(t) = -2A(t)\lambda(t)\mathrm{Im}\langle\psi(t)|W\mu|\psi(t)\rangle, \tag{2.28}$$

where $A(t)$ is a positive function of time and the constant factor 2 is introduced for convenience. [The π-phase shifted pulse of Eq. (2.28) always gives a negative value to the time derivative.] Since this expression has the same form as Eq. (2.12), we can see that our scheme includes their pulse-shaping method as a special case of $g(t)=0$. Our method, on the other hand, has the freedom to choose $g(t)$ different from zero ($g(t)$ can be chosen anything at least in principle), and therefore the present method is more general than that by Kosloff *et al.* Furthermore, our method explicitly shows the relation between the local and optimal control pulses. This is important since any approximated treatments must be related to the optimal control method as long as they share the common goal of optimal field design.

Our pulse design needs a known function, $g(t)$, to determine the control pulse. In this context, our method has a similarity to the tracking problem,[30–33] which is the inverse quantum-mechanical control of molecules. In Eq. (2.26), by replacing the functional $F[\langle W(t)\rangle]$ with a known function of time and then solving for $E(t)$, we obtain the inverse control solution. This is a simple case study of tracking. Rabitz and co-workers[32] calculated control fields by minimizing a cost functional that contains terms designed to minimize the error between the objective and actual tracks and also minimize the field energy. They performed calculations locally in time to retain the local nature of the tracking method. Thus, it is not clear what kind of approximation and/or assumption are needed to directly derive their expressions when starting with the optimal control method. Contrary to this, our ''known function'' gives a possible solution to the optimal control problem, and therefore our scheme has a direct relation to the optimal control method. In this sense, our scheme may be regarded as another type of tracking.

III. APPLICATION TO POPULATION CONTROL

In this section and the next section, we will show numerical applications using the control pulse given by Eq. (2.12) [or Eq. (2.20)]. Since the control pulse is written in terms of the wave function, there appears a nonlinear term with respect to the wave function in the Schrödinger equation. Through this nonlinear term, feedback for the control pulse is incorporated. In order to solve the coupled equations, Eqs. (2.6) and (2.12), we can use a simple algorithm because no iteration is required in the local control method. The control pulse at time t is calculated using the wave function at time t by Eq. (2.12). Then by substituting $E(t)$ into the Schrödinger equation Eq. (2.6), the wave function is propagated from t to the next time step $t+\Delta t$. We examined the numerical stability by slightly changing the parameter values, and we found that our numerical procedure sometimes becomes unstable in the presence of high-order nonlinear terms. However, when we chose $\lambda(t)=1$ $[F[\langle W(t)\rangle]=\langle W(t)\rangle]$ and $A(t)=A$ (constant), such instability was not observed. Thus, we only consider this case. In this case, the electric field amplitude is proportional to parameter A. Thus, we may call A an amplitude parameter.

In the following, dimensionless energy and time are utilized, while the electric field amplitude and the transition moment are measured in units of V/m and Debye, respectively. For this purpose, we introduce a unit energy ϵ_0, which is measured in units of cm^{-1}. The electric field amplitudes show the magnitude when the unit energy is set to $\epsilon_0=1\ \mathrm{cm}^{-1}$. If $\epsilon_0=300\ \mathrm{cm}^{-1}$ is chosen, then 5×10^5 V/m amplitude, for example, should read $300\times(5\times10^5\ \mathrm{V/m})=1.5\times10^8$ V/m.

A. Two-level system

To see how the control pulse is created by the local control method with the algorithm described above, we apply it to a two-level system. This system is specified by states $|1\rangle$ and $|2\rangle$ whose energy eigenvalues are given by $\hbar\omega_1$ and $\hbar\omega_2$, respectively. As a simple example, we consider the population inversion, assuming that the system is initially in the ground state $|1\rangle$. For this purpose, we use the target operator consisting of two projectors with weight factors w_1 and w_2,

$$W=|1\rangle w_1\langle 1|+|2\rangle w_2\langle 2|. \tag{3.1}$$

According to the algorithm, the control pulse at time t is written as

$$E(t)=-2A\ \mathrm{Im}\langle\psi(t)|W\mu|\psi(t)\rangle, \tag{3.2}$$

where $\mu=|2\rangle\mu_{21}\langle 1|+|1\rangle\mu_{21}^*\langle 2|$ is a transition moment operator. To obtain an analytical expression of the control pulse, we expand the wave function in terms of the eigenstates

$$|\psi(t)\rangle=C_1(t)e^{-i\omega_1(t-t_0)}|1\rangle+C_2(t)e^{-i\omega_2(t-t_0)}|2\rangle \tag{3.3}$$

and substitute Eq. (3.3) into Eq. (3.2). The control pulse is then expressed as

$$E(t)=-2A|C_1(t)||C_2(t)||\mu_{21}|(w_2-w_1)\times\sin[\omega_{21}(t-t_0)+\theta(t)], \tag{3.4}$$

where the phase $\theta(t)$ comes from the expansion coefficients and the transition moment. Since the interaction picture removes the rapidly oscillating phase associated with the energies $\hbar\omega_1$ and $\hbar\omega_2$ from the expansion coefficients, $\theta(t)$ is a slowly varying function of time. [In the weak-field limit, the phase $\theta(t)$ has a time-independent value.] From this example, we can see that the frequency of the control pulse corresponds to the transition frequency $\omega_{21}=\omega_2-\omega_1$ and that the envelope function of the pulse is determined by the expansion coefficients, i.e., the system dynamics.

Since the time-dependence of the envelope function well illustrates the feedback mechanism, we consider the expansion coefficients at the next time step $t+\Delta t$. For a small time interval Δt, these coefficients are approximated by

$$|C_j(t+\Delta t)|=|C_j(t)|+\delta|C_j|, \qquad (j=1,2). \tag{3.5}$$

Then using the normalization condition

$$\sum_{j=1,2}|C_j(t)|^2=\sum_{j=1,2}|C_j(t+\Delta t)|^2=1 \tag{3.6}$$

we can obtain the relation

$$|C_1(t+\Delta t)||C_2(t+\Delta t)|-|C_1(t)||C_2(t)|=\delta|C_2||C_1(t)|\left[1-\frac{|C_2(t)|^2}{|C_1(t)|^2}\right], \tag{3.7}$$

where $\delta|C_2|>0$ in the excitation process. This indicates that when the population in the ground state $|1\rangle$ is more (or less) than that in the excited state $|2\rangle$, the envelope function becomes larger (or smaller).

To confirm this result numerically, we calculate the control pulse and the population that are shown in Fig. 1. In this calculation, frequencies are measured in units of the frequency difference $\omega_{21}=\omega_2-\omega_1$. The transition moment is set to $\mu_{21}=1.0$ Debye. We employ the amplitude parameter $A=3.0\times10^5$ and the weight factors $w_1=0$ and $w_2=1.0$. The time evolution of the molecular system is calculated by the Runge–Kutta method. Our purpose here is to completely transfer the population initially in the ground state to the

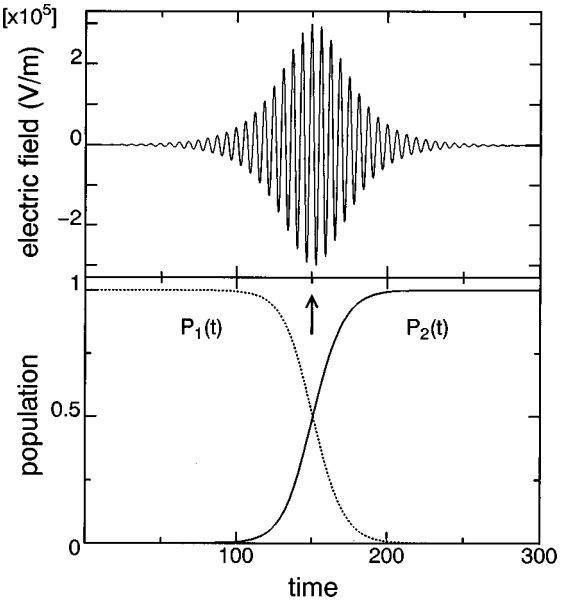

FIG. 1. Two-level system. Control pulse as a function of time (upper figure) and time-evolution of population (lower figure). In the lower figure, the solid (dotted) line represents the population of level $|2\rangle(|1\rangle)$. The arrow indicates the time when both levels are equally populated.

excited state. Thus, the control pulse is a so-called π-pulse since it has a resonant frequency of ω_{21}. For the pulse envelope function, it increases until both states are equally populated, as indicated by the arrow in Fig. 1). After that, the envelope function becomes smaller and smaller as predicted by Eq. (3.7).

B. Three-level system

In this subsection, we consider a population inversion in a three-level system. This model has a ground state $|1\rangle$, an intermediate state $|2\rangle$ and a final state $|3\rangle$ whose energies are given by $\hbar\omega_1$, $\hbar\omega_2$, and $\hbar\omega_3$, respectively. The transition moment operator is assumed to have a form of

$$\mu=|3\rangle\mu_{32}\langle 2|+|2\rangle\mu_{21}\langle 1|+\text{h.c.} \tag{3.8}$$

Starting with the ground state at initial time t_0, we calculate the control pulse that transfers the population to the final state. For this purpose, we use a target operator

$$W=|1\rangle w_1\langle 1|+|2\rangle w_2\langle 2|+|3\rangle w_3\langle 3|. \tag{3.9}$$

As can be anticipated from the two-level system, the control pulse includes two frequency components corresponding to the transition frequencies ω_{21} and ω_{32}. If there is a difference between these transition frequencies, there appears a modulation in the control pulse. Thus, it is expected that the pulse shape is characterized by the frequency difference $\Delta=\omega_{21}-\omega_{32}$. For this reason, we consider two typical cases. One of them is called a strong-field case, where population inversion is completed before $1/\Delta$. In the other case, called a medium-field case, the population inversion is completed after $1/\Delta$, and the control pulse is therefore considerably modulated by the frequency difference. Here, we would like to stress again that the pulses in both cases cause population inversion, and they are therefore ''strong'' pulses in the usual sense.

The pulse shape is determined by the parameters of the target operator, w_1, w_2, and w_3, and the amplitude parameter A. Change in parameter values will alter the structure of the objective functional J, which may lead to a different type of control pulse. For example, a larger value of A makes the contribution from the penalty term to the objective functional less important and allows a more intense laser pulse. To illustrate this, fixed values $w_1=0$, $w_2=1.0$, and $w_3=2.0$ are chosen, while two values of A are used to adjust the field intensity. In the following examples, the transition frequency ω_{21} is chosen as the unit frequency, i.e., $\omega_{21}=1$.

First let us consider the medium-field case where an amplitude parameter is set to $A=5.0\times10^7$. Since we can expect that almost complete population inversion can be realized by an appropriate choice of the parameters, we examine the ''quality'' of our choice by comparing numerical results with analytical solutions. In the special case of $\Delta=0(\omega_{21}=\omega_{32})$, the time-evolution of the system interacting with the pulse

$$E(t)=E_0(t)\cos(\omega t+\theta) \tag{3.10}$$

can be determined analytically, provided that the frequency of the pulse ω is equal to ω_{21} and that the RWA is valid. In this case, we need not consider a time-ordering of operators because of the commutation relation

$$[V_I^{t_1}(t_1),V_I^{t_2}(t_2)]=0, \quad (t_1\neq t_2), \tag{3.11}$$

where the interaction representation is defined by

$$V_I^t(t)=\exp[iH_0(t-t_0)/\hbar]V^t\exp[-iH_0(t-t_0)/\hbar]. \tag{3.12}$$

The wave function at time t can be obtained after minor algebra. From this expression, we have the population of the state $|3\rangle$ at time t,

$$P_3(t)=\frac{\eta}{(1+\eta)^2}\left[1-\cos\frac{\sqrt{1+\eta}}{2}S(t)\right]^2, \tag{3.13}$$

where

$$\eta=|\mu_{21}/\mu_{32}|^2 \tag{3.14a}$$

and the pulse area

$$S(t)=\frac{|\mu_{32}|}{\hbar}\int_{t_0}^{t}d\tau E_0(\tau). \tag{3.14b}$$

Equation (3.13) means that the maximum value of the population of the highest state at a controlling time t_f is given by $P_3(t_f)=4\eta/(1+\eta)^2$ when the pulse area is adjusted to $S(t_f)=2\pi/\sqrt{1+\eta}$. We calculated $P_3(t_f)$, employing several values of η, and found that the control pulses always re-produce the theoretically predicted maximum values within 1%–2% errors. This implies that the target operator and the amplitude parameter employed here are suitable for specifying the objective state.

To see how the energy level structure of the system affects the pulse shapes, we calculated the control pulses for three cases of transition energy differences, $\Delta=0$, 0.1, and

0.3. With the transition moment, $\mu_{21}=\mu_{32}=1.0$ Debye is assumed. The numerical results are shown in Figs. 2(a)–2(c), in which the upper figures show the control pulse. The lower figures show the time-evolution of the population of the state $|j\rangle$ which is denoted by $P_j(t)$ $(j=1,2,3)$. We can see from Fig. 2(a) [$\Delta=0$] that the calculated pulse has a pulse area of nearly $\sqrt{2}\pi$. In fact, the analytical result given by Eq. (3.13) shows that for resonant excitation in the RWA, any pulse that realizes 100% population inversion has a pulse area of $S(t_f)=\sqrt{2}\pi$ at a control time. That is, the local control method predicts one of the $\sqrt{2}\pi$-pulses.

If the excitation occurs in a sequential way, i.e., the ground state population is excited to the intermediate state and then this excited population is transferred to the final state, the pulse has an area of 2π. The pulse area of $\sqrt{2}\pi$ in the case of $\Delta=0$ thus means that the simultaneous excitation process considerably contributes to the population inversion. Because of this coherent contribution, the population of the intermediate state shows a small peak [Fig. 2(a)]. By contrast with the simple pulse shape in the case of $\Delta=0$, when $\Delta\neq 0$, the control pulse has an interference structure that destroys the coherent excitation process. Such numerical examples are shown in Fig. 2(b) ($\Delta=0.1$) and Fig. 2(c) ($\Delta=0.3$). In both cases, the control pulses transfer almost 100% of the population from the ground state to the final state. In the case of $\Delta=0.1$, the control pulse has two temporal peaks due to the modulation, and by this interference, the population $P_2(t)$ transiently grows to 0.75 [Fig. 2(b)]. As the value of the transition energy difference Δ increases, the interference becomes more prominent, and this finally divides the control pulse into two π-pulses [Fig. 2(c)]. In this limiting case, the excitation process is described by the sum of the two independent transitions, from $|1\rangle$ to $|2\rangle$ and from $|2\rangle$ to $|3\rangle$. The time evolution of the population also confirms this sequential excitation process.

Next, consider the case of $A=2.0\times 10^8$, which corresponds to the strong-field case. In Fig. 3(a), the control pulse in the case of $\Delta=0.08$ is represented by the solid line. For reference, we also show the control pulse in the case of $\Delta=0$ by the dotted line. These pulses have the same structure in the first half, since we have assumed the fixed frequency $\omega_{21}=1$ for the first transition from the ground state to the intermediate state. After completing the first transition, the pulse in the case of $\Delta=0.08$ is slightly modulated by the frequency difference, i.e., the control pulse is a chirped pulse.[34,35] In Fig. 3(b), the solid line shows the time-evolution of the population of each state. Even in the presence of the transition energy difference, about 95% of the population is transferred to the final state. To illustrate the importance of chirping, we also calculated the population using the pulse obtained in the case of $\Delta=0$ instead of the control pulse. This time-evolution of the population is presented by the dotted line in Fig. 3(b). Since these pulses have the same frequency in the first half, there is little difference between the time-dependent behaviors of their population until $t=50$. After that, the pulse obtained in the case of $\Delta=0$ partially stimulates emission because of the frequency mismatch. Although the difference between two pulses appears to be very small [Fig. 3(a)], the result shows that the yield is reduced to 72%. We therefore conclude that chirping is essential to enhance the population inversion.

IV. APPLICATION TO WAVE PACKET CONTROL

Besides population control, there are several physically interesting objectives for quantum control, and wave packet shaping is one of them.[9,11–15,19,20] The purpose of this control is to localize atoms to specify a molecular geometry in the configuration space. To illustrate wave packet control, we apply the local control method to a molecule with two electronic potential energy surfaces (PESs). Our purpose here is to find a pulse that creates a localized wave packet in the electronically excited state at a given position at a given time.

A. Displaced harmonic oscillator model

We adopt a two-electronic-state model with harmonic potentials, which is schematically illustrated in Fig. 4. These harmonic oscillators are represented by a dimensionless coordinate and have a dimensionless unit frequency. The molecular Hamiltonian is given by

$$H_0=|g\rangle h_g\langle g|+|e\rangle(h_g+\omega_{\rm el})\langle e|, \tag{4.1}$$

with

$$h_g=\tfrac{1}{2}p^2+\tfrac{1}{2}q^2 \tag{4.2a}$$

and

$$h_e=\tfrac{1}{2}p^2+\tfrac{1}{2}(q-\delta)^2, \tag{4.2b}$$

where h_g and h_e are vibrational Hamiltonians in the electronically ground $|g\rangle$ and excited states $|e\rangle$, respectively. The potential displacement between them is set to $\delta=3.0$. For a dimensionless electronic energy, $\omega_{\rm el}$, the introduction of a rotating frame allows us to use any value as long as the RWA is valid. Here, it is chosen as $\omega_{\rm el}=50$. We neglect the nuclear-coordinate dependence of the electric transition moment, and we use $\mu_{eg}=1.0$ Debye. The initial state of the molecule is assumed to be in the lowest vibrational state in the ground electronic state $|g0\rangle$. The wave function is expanded in terms of the vibrational states in both electronic states. Then the Runge–Kutta method is used to determine the time-evolution.

As an objective state, we choose a localized Gaussian function with a zero average velocity, $f_G(q)$ on the excited electronic PES. This function is characterized by a probability distribution function ($f_G(q)=|\langle q|f_G\rangle|$),

$$[\langle q|f_G\rangle]^2=\frac{1}{\sqrt{2\pi}\sigma}\exp\left[-\frac{(q-q_0)^2}{2\sigma^2}\right] \tag{4.3}$$

with two parameters, q_0 (central position) and σ (distribution width). Since our purpose is to yield a wave packet on the excited PES that has maximum overlap with the target distribution $|f_G\rangle$ at a control time, the projector $|f_G\rangle\langle f_G|\otimes|e\rangle\times\langle e|$ is a natural choice for the target operator. However, we are now restricted ourselves to the special case where the control pulse is given by Eq. (2.12) [or Eq. (2.20)], and this requires that the target operator should commute with the molecular Hamiltonian [see Eq. (2.9)]. If the target operator

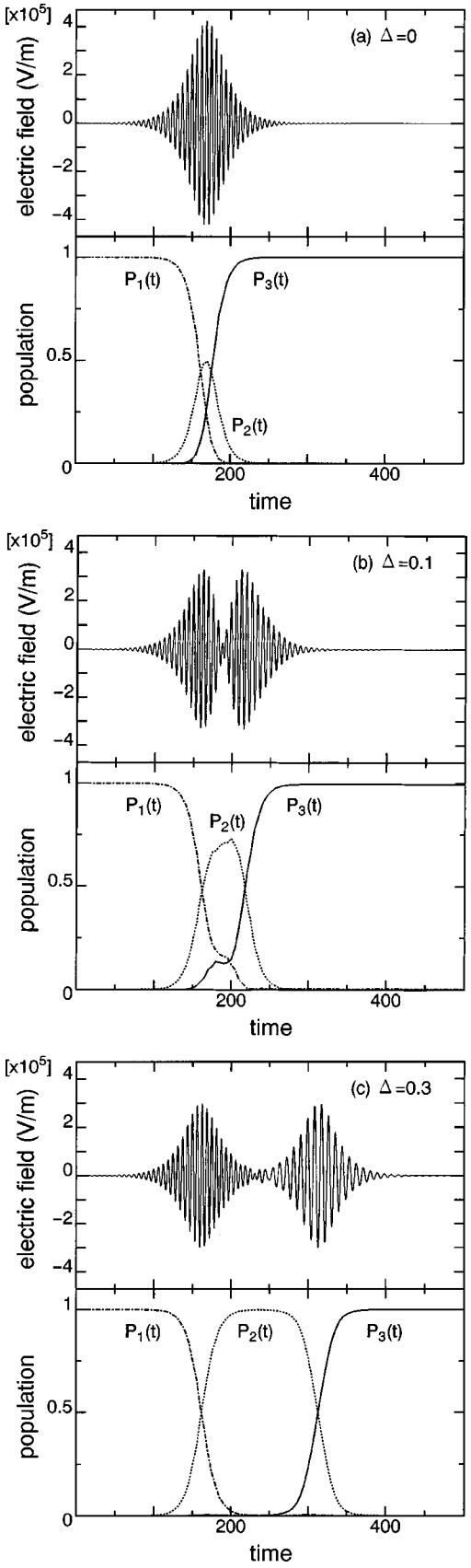

FIG. 2. Three-level system in the medium-field case. Control pulse as a function of time (upper figure) and time-evolution of the population of each level (lower figure). The population of level $|1\rangle$ is $P_1(t)$ (dot–dashed line), that of $|2\rangle$ is $P_2(t)$ (dotted line), and that of $|3\rangle$ is $P_3(t)$ (solid line). The transition energy differences are set to (a) $\Delta=0$, (b) $\Delta=0.1$, and (c) $\Delta=0.3$.

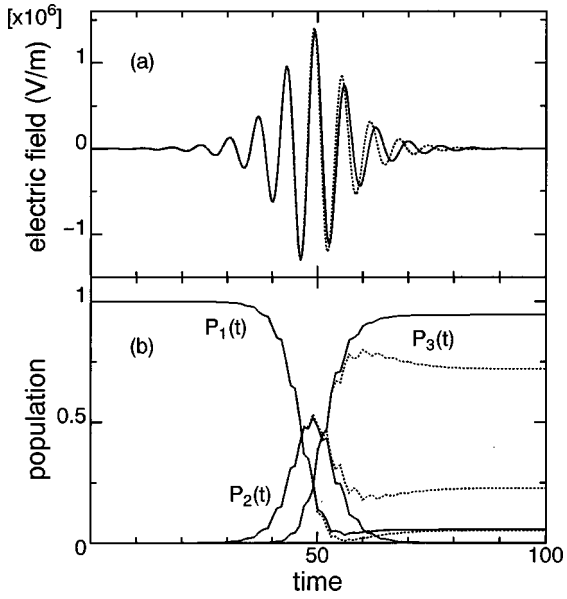

FIG. 3. Three-level system in the strong-field case. (a) Control pulses as functions of time in the cases of transition energy difference $\Delta=0.08$ (solid line) and $\Delta=0$ (dotted line). (b) Time-evolution of the population for the system with $\Delta=0.08$. The solid and dotted lines show those under the irradiation of pulses obtained in the cases of $\Delta=0.08$ and $\Delta=0$ in (a), respectively.

includes the above-mentioned projector, then the target operator does not commute with the vibronic Hamiltonian h_e.

To avoid this difficulty, we calculate the control pulse by backward propagation from the objective Gaussian to the initial state $|g0\rangle$. Thus, the formal target state is the initial state $|g0\rangle$, and the formal initial state is the objective Gaussian. The information on the target Gaussian is included through this formal ''initial'' state. By backward propagation, we can use a simple target operator,

$$W=|e\rangle w_e\langle e|+|g0\rangle w_{g0}\langle g0|+\sum_{v(v\neq 0)}|gv\rangle w_{gv}\langle gv|, \tag{4.4}$$

which commutes with the molecular Hamiltonian in Eq. (4.1). Sine we have to avoid populating the vibrationally

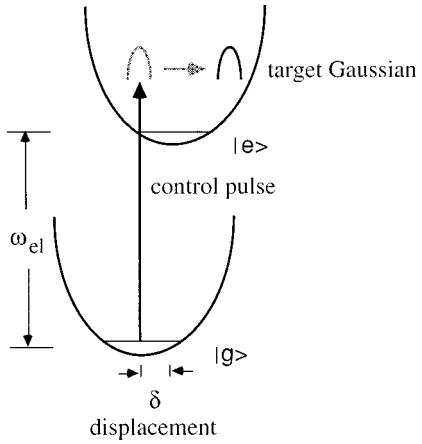

FIG. 4. Schematic illustration of wave packet shaping with a displaced harmonic oscillator model.

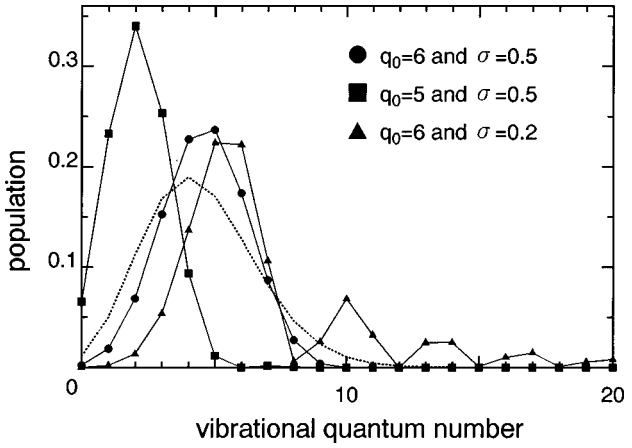

FIG. 5. Vibrational-state distribution included in the target Gaussians in the cases of $(q_0,\sigma)=(6,0.5)$ (full circles), $(q_0,\sigma)=(5,0.5)$ (full squares), and $(q_0,\sigma)=(6,0.2)$ (full triangles). The dotted line shows the vibrational quantum number dependence of the Franck–Condon factors between the lowest state $|g0\rangle$ and the vibrational states $\{|ev\rangle\}$.

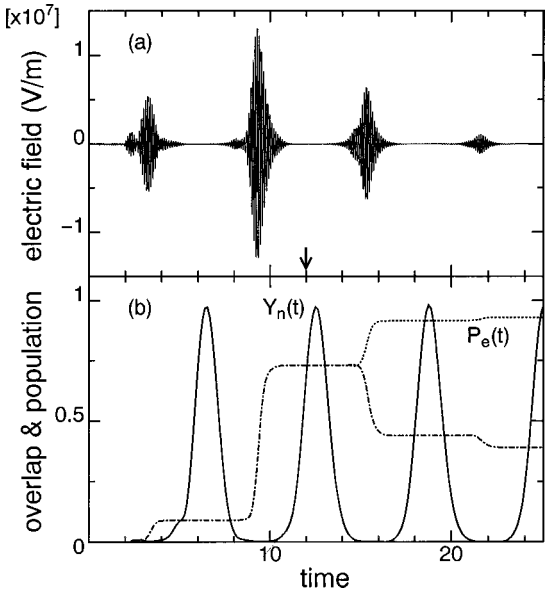

FIG. 6. Wave packet shaping for the target Gaussian with $(q_0,\sigma)=(6,0.5)$. (a) Control pulse as a function of time, and (b) time-evolution of normalized overlap integral $Y_n(t)$ [Eq. (4.5b), solid line] and that of excited population $P_e(t)$ [Eq. (4.5a), dotted line]. The dot–dashed line shows the time-evolution of the excited population when the phase of the control pulse is shifted by π at time $t=12$ (indicated by an arrow).

excited states in the ground electronic state $|gv\rangle$ $(v\neq 0)$, we use the values of $w_e=0$, $w_{g0}=0.5$, and $w_{gv}=-0.5$. $(v\neq 0)$. The minus values for w_{gv} give penalty terms. The numerically obtained pulse is substituted back into the Schrödinger equation to confirm that the calculated pulse actually works as a control pulse, i.e., it gives a high product yield. We check the stability of the solution by slightly changing the values of input parameters. The time-evolution of the population and the wave packet motion are obtained by forward-propagation calculation.

In the first example, the target parameters q_0 and σ are set to $q_0=6$ and $\sigma=0.5$, and the amplitude parameter is set to $A=3.0\times 10^7$. This target Gaussian has a $\frac{1}{2}$ narrower probability distribution width than the initial ground state $|g0\rangle$. In Fig. 5, the distribution of the vibrational states included in this Gaussian is represented by full circles. For reference, the dotted line shows the Franck–Condon factors between the initial state $|g0\rangle$ and the vibrational states in the electronic excited states $\{|ev\rangle\}$. As can be seen from this figure, the vibrational distribution of the target Gaussian is similar to that of the Franck–Condon factors.

Figure 6(a) shows the calculated control pulse. Three-pulse sequences are needed to de-excite the wave packet to the lowest state in the backward propagation because of the broad energy distribution of the target Gaussian. There may be a better choice of parameter values that makes it possible to complete the de-excitation by one pulse; however, we could not find such a parameter set in this time range. If we denote ω as the oscillator frequency and assume $\omega=150$ cm^{-1}, for example, then the control time $t_f=25$ corresponds to $t_f=0.88$ ps. Since the target Gaussian has a similar form to that of the Franck–Condon wave packet, each pulse sequence is represented by a simple pulse.

In Fig. 6(b), the dashed line represents the time-evolution of the population created on the excited PES, which is defined by

$$P_e(t)=|\langle e|\phi(t)\rangle|^2=\langle\phi_e(t)|\phi_e(t)\rangle. \tag{4.5a}$$

The solid line denotes the absolute value of the overlap integral of the wave function with the target Gaussian

$$Y_n(t)=\frac{|\langle\phi_e(t)|f_G\rangle|}{\sqrt{P_e(t)}}. \tag{4.5b}$$

This overlap integral is normalized with respect to the population on the excited PES. We can see that more than 90% of the population is transferred to the excited state and that the control pulse creates a well-shaped wave packet whose overlap integral with the target is $Y_n(t_f)=0.98$.

Comparing the control pulse with the time-evolution of the overlap integral, we can see that each pulse sequence is in accord with the wave packet motion. This is because the control pulse makes use of the constructive interference to efficiently excite the population, i.e., to save the pulse energy. The pulse sequences thus have a definite phase relation to each other. This mechanism has been reported in the weak-field regimes in which the excited population is created linearly in proportion to the laser intensity.[13–15] To illustrate the phase effect in strong-field regimes, we change the phase of the control pulse by π at $t=12$ [indicated by the arrow in Fig. 6(a)] and then calculate $P_e(t)$. The π-phase shifted pulse which can cause the largest destructive interference gives the smallest amount of excited population if the phase relation plays an important role. The numerical result is given by the dot–dashed line in Fig. 6(b). As expected, the π-phase shifted pulse causes destructive interference, which results in a considerable decrease in $P_e(t_f)$. Therefore, the importance of the phase relation in pulse sequences is confirmed even in the strong-field case where population inversion occurs. An interesting point is that the control pulse is calculated by backward time-propagation, although its features are consistently interpreted on the basis of the forward

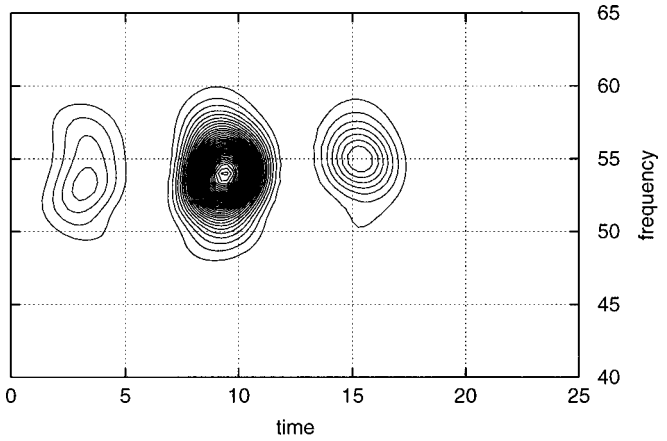

FIG. 7. Contour map of the time- and frequency-resolved spectrum of the control pulse in Fig. 6(a).

time-propagation picture. This, of course, originates from the time reversibility of the Schrödinger equation. Our calculation, thus, explicitly shows that the phase of the pulse is also important in the case of an optical transition from a wave packet to an eigenstate, i.e., stimulated emission process.

To discuss the pulse structure in detail, we calculate the time- and frequency-resolved spectrum. This spectrum is defined by

$$S(\omega,t)=\left|\int_{-\infty}^{\infty} d\tau H(\tau-t,T)E(\tau)E(\tau)e^{i\omega t}\right|^2, \tag{4.6}$$

where $H(\tau,T)$ is a window function with time-resolution T. Here, we adopt the Blackman window function which is given by

$$H(\tau,T)=0.42+0.50\cos\left(\frac{2\pi}{T}\tau\right)+0.08\cos\left(\frac{4\pi}{T}\tau\right), \tag{4.7}$$

when $|\tau|\leqslant T/2$ and is set to zero when $|\tau|>T/2$.

The calculated spectrum is shown in Fig. 7, in which the fourth small pulse does not appear in the present intensity scale. All contour maps have simple forms. Although the central frequency of each pulse sequence slightly shifts from low- to high-frequency components in time, each sequence has a broad frequency distribution that covers all frequencies needed for the transitions. A frequency of 55 corresponds to transition energy from $|g0\rangle$ to $|e5\rangle$, which is the largest vibrational component in the target Gaussian. A frequency of 54 corresponds to that to $|e4\rangle$, which has the largest Franck–Condon factor. The frequency components below $\omega_{\mathrm{el}}=50$ cause transitions from and/or to the excited vibrational states in the ground excited state to and/or from the target Gaussian.

In the first example, the distribution of the vibrational states included in the target Gaussian is closely correlated with that of the Franck–Condon factors. Thus, it is easy to realize a high achievement by a simple control pulse. In the next example, we consider the case where there is a large discrepancy between them. For this purpose, we adopt the target Gaussian with $q_0=5$ and $\sigma=0.5$, whose vibrational-state distribution is shown by full squares in Fig. 5. To adjust

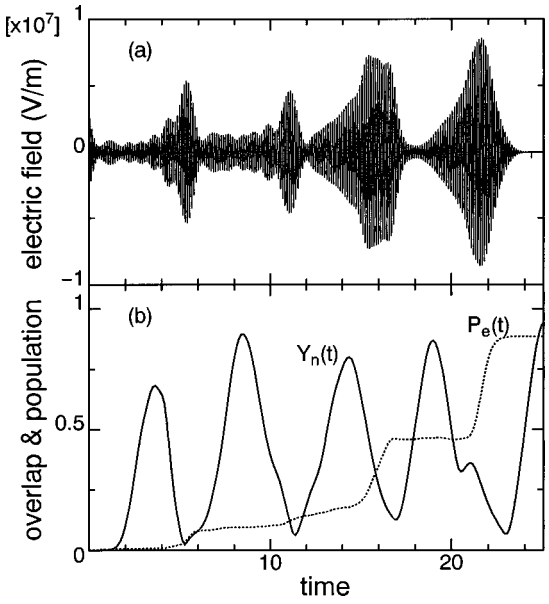

FIG. 8. Wave packet shaping for the target Gaussian with $(q_0,\sigma)=(5,0.5)$. (a) Control pulse as a function of time, and (b) time-evolution of normalized overlap integral $Y_n(t)$ (solid line) and that of excited population $P_e(t)$ (dotted line).

the laser intensity, the amplitude parameter is set to $A=6.0\times10^7$, while the other parameters are assumed to have the same values as those used in the first example. Figure 8 shows (a) the control pulse, and (b) time-evolution of the overlap integral (solid line) and that of excited population (dotted line). Although the control pulse has a complicated structure, we still have a good control achievement, $P_e(t_f)=0.89$ and $Y_n(t_f)=0.94$.

From Fig. 8(b), we can see that the last two pulse sequences whose temporal peaks are around $t=15$ and $t=22$ control about 80% of the population. The time- and frequency-resolved spectrum in Fig. 9 shows that these pulse sequences are up-chirped pulses. Before giving physical interpretation to this chirped structure, we discuss it from a

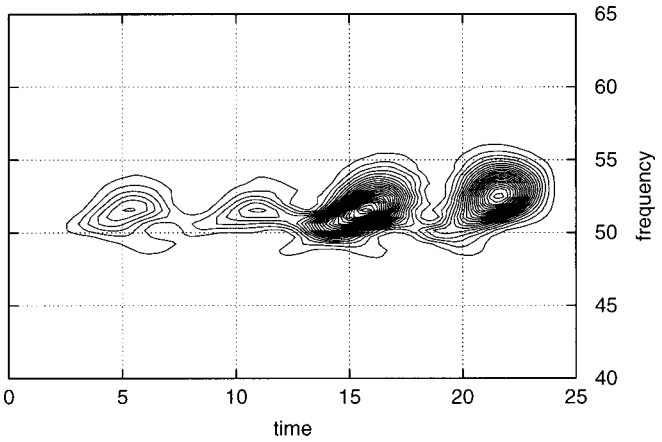

FIG. 9. Contour map of the time- and frequency-resolved spectrum of the control pulse in Fig. 8(a).

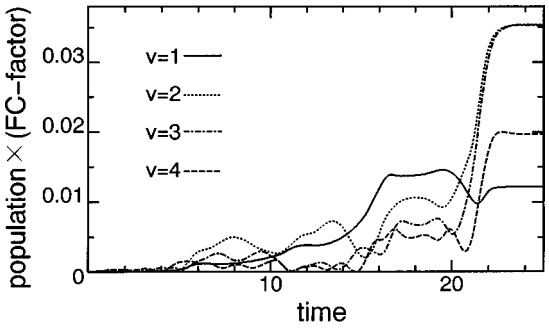

FIG. 10. Time-dependence of $\{a_v(t); v=1,2,3,4\}$ which is defined by Eq. (4.8).

numerical viewpoint based on the vibrational-eigenstate picture. As seen in Sec. III, the amplitude of each frequency component included in a pulse is determined by the magnitudes of the transition moments and the population of the vibrational states. To estimate the amplitude, it is convenient to introduce a property $a_v(t)$, which is defined by

$$a_v(t)=|{}_g\langle 0|v\rangle_e|^2 P_{ev}(t). \tag{4.8}$$

This is a product of the Franck–Condon factor with the population of the vth vibrational state $P_{ev}(t)$. Roughly speaking, the amplitude at time t associated with the transition from $|ev\rangle$ to $|g0\rangle$ is proportional to $a_v(t)$. Figure 10 shows the calculated results for the vibrational states $v=1$, 2, 3, and 4. Using this, we first discuss the structure of the pulse sequence with the temporal peak at $t\sim 22$, whose spectrum is shown in Fig. 9. For convenience, let us look at the control pulse inversely, i.e., from $t_f=25$ to $t_0=0$. In the backward calculation, the control pulse transfers the target Gaussian to the lowest state. Since $a_{v=2}(t_f)$ and $a_{v=3}(t_f)$ are dominant at time t_f, this pulse sequence tries to de-excite the $v=2$ and $v=3$ states in the first part of it (in the backward sense). Since the high vibrational states ($v\geqslant 2$) have large Franck–Condon factors (Fig. 5), they are efficiently de-excited to the lowest state. On the other hand, the $v=1$ state slightly changes its population because of the small Franck–Condon factors. Thus, through this de-excitation process, $\{a_v(t);\ v=2,3,4\}$ become smaller and $a_{v=1}(t)$ becomes more dominant (Fig. 10). This gradually decreases high-frequency components and increases low-frequency components. The de-excitation process also transfers the part of population to the vibrationally excited states in the electronic ground state, in which we put penalty weights. Thus, the last part of the pulse sequence whose frequency is below $\omega_{\mathrm{el}}=50$ is used to remove this population. Since all theses transitions occur sequentially within the pulse sequence, the control pulse has a chirped structure.

For the pulse sequence with a temporal peak at $t\sim 15$, the central frequency is first tuned to around 51.5, since $a_{v=1}(t)$ and $a_{v=2}(t)$ have large values. Then the $v=2$, 3, and 4 states are quickly transferred to the lowest state because of their large Franck–Condon factors, so that $a_{v=1}(t)$ becomes dominant around $t=15$. This causes a low-frequency shift in the pulse sequence and makes the structure up-chirped. Since the pulse sequence at $t\sim 22$ removes most

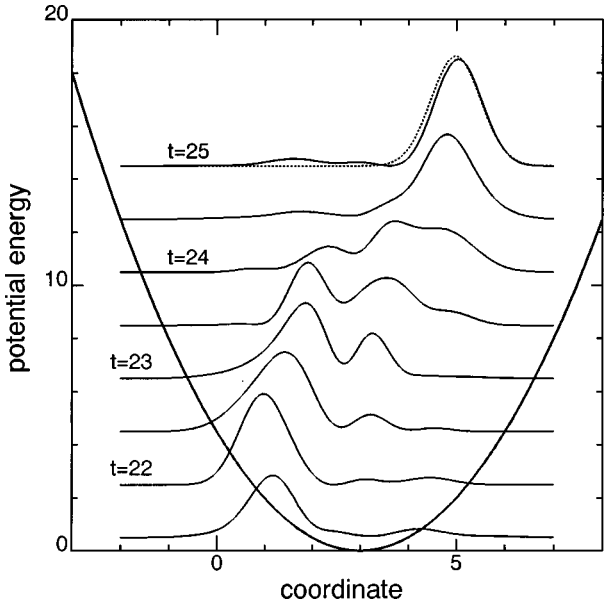

FIG. 11. Snapshots of the probability density $|\langle q|\phi_e(t)\rangle|^2$ for the last half period with an excited harmonic potential. The dotted line shows the target Gaussian.

of the high vibrational states ($v\geqslant 2$), the pulse sequence at $t\sim 15$ shows a weaker chirping than that at $t\sim 22$. After these two pulse sequence, the wave packet is destroyed and spread over the potential well because of the lack of several vibrational states. By this dephasing, the periodic structure of the control pulse gradually disappears. Our pulse-shaping method always tries to realize as high an achievement as possible, even using small values of the transition moments. Since several frequency components appear simultaneously with relatively low intensities, we see modulations in the time range of $0\leqslant t\leqslant 12$. Such modulations also give a complicated structure to the control pulse in Fig. 7(a).

To give physical interpretation to the control pulse, we calculated the wave packet motion on the excited PES for the last half period, which is shown by the solid line in Fig. 11. Here the wave packet is defined by a square of the wave function $|\langle q|\phi_e(t)\rangle|^2$. For reference, the target Gaussian is shown by the dotted line The characteristic of the wave packet motion is that it has two spatial peaks at the time when the wave packet is passing around the center of the excited PES. When the first peak reaches the turning point of the potential and goes back, the second peak meets this reflected component near the turning point. Since the control pulse causes constructive interference between these peaks, the wave packet is sharpened so as to have a large overlap with the target Gaussian. Contrary to an anharmonic system, the harmonic system does not have a degree of freedom originating from frequency differences. Thus, the local control pulse utilizes the constructive interference between the advanced and delayed components for squeezing the wave packet. Therefore, each pulse sequence consists of smaller pulse trains whose temporal separation corresponds to the two peaks in the wave packet. A chirped pulse can be regarded as a sum of pulse sequences with different frequen-

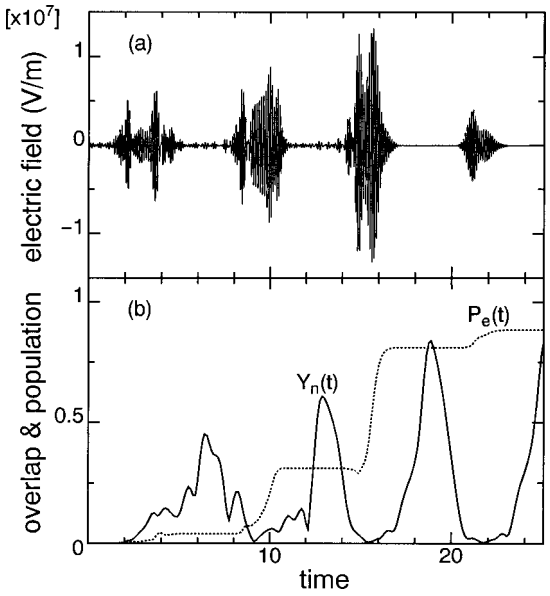

FIG. 12. Wave packet shaping for the target Gaussian with $(q_0,\sigma)=(6,0.2)$. (a) Control pulse as a function of time, and (b) time-evolution of normalized overlap integral $Y_n(t)$ (solid line) and that of excited population $P_e(t)$ (dotted line).

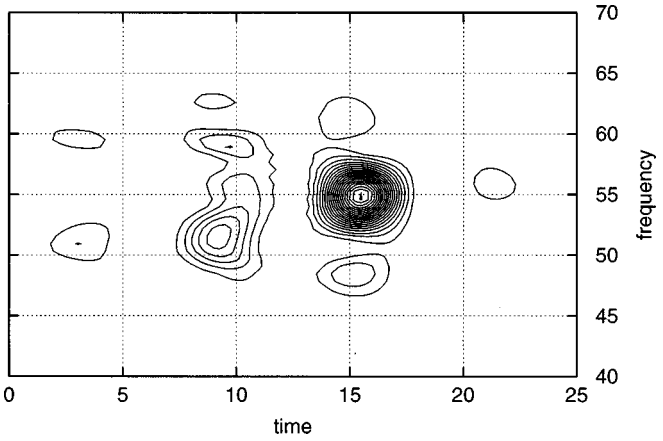

FIG. 13. Contour map of the time- and frequency-resolved spectrum of the control pulse in Fig. 12(a).

cies, whose temporal separation is imperfect because of the short temporal width of the pulse. This is the reason why the pulse sequences have chirped structures. This wave packet-shaping mechanism is more clearly shown by the next example.

In the final example, we deal with the target Gaussian with a central position $q_0=6$ and a narrow distribution width $\sigma=0.2$. This target Gaussian is composed of many vibrational states whose distribution is given by full triangles in Fig. 5. Since some of the vibrational states have small values of the Franck–Condon factors, control is expected to be a difficult task. The calculated control pulse appears in Fig. 12(a), while Fig. 12(b) shows the time-evolution of normalized overlap $Y_n(t)$ (solid line) and that of the excited population $P_e(t)$ (dotted line). We can see from Fig. 12(a) that the control pulse has four well-separated pulse sequences that consist of smaller pulse trains. From a physical viewpoint, the control pulse tries to squeeze the wave packet using the constructive interference between the advanced and delayed components of it. For this purpose, successive excitation by the small pulse trains are needed to create a wave packet that has two components separated in time. The constructive interference sharpens the wave packet to have the normalized overlap of $Y_n(t_f)=0.84$ at the control time [Fig. 12(b)]. Since the target Gaussian includes the optically inactive vibrational states, the control pulse achieves $P_e(t_f)=0.88$ population transfer to the electronically excited state.

To discuss the structure of each pulse sequence in detail, we calculated the time- and frequency-resolved spectrum, which is shown in Fig. 13. Again, it is convenient to analyze the structure using $a_v(t)$ [Eq. (4.8)] and inversely in time. A large value of $a_v(t)$ implies that the vth vibrational state is optically active and has a large population. Thus, the control pulse can efficiently transfer its population with small energy utilizing a large value of the Franck–Condon factor. Since our method locally optimizes the dynamics, the control pulse first de-excites the vibrational states around $v=5$ because of large values of $a_v(t_f)$. This is the reason why the pulse sequences with temporal peaks at $t\sim 22$ and $t\sim 16$ have a central frequency of ~ 55. Since this de-excitation process removes the vibrational states around $v=5$ from the target Gaussian, the control pulse tries to de-excite the remaining states that are distributed around $v=2$ and $v=10$ (and higher). This is the reason why the pulse sequences at $t\sim 10$ and $t\sim 3$ have a broad and separate frequency distribution. The distribution width is large enough to cause modulation within pulse sequences, which results in complicate structures. In the second example, the pulse sequence is a chirped pulse, while in the final example, it consists of small pulse trains. This difference can be understood by the relation between the temporal width and the frequency distribution width, as we showed in Sec. III B.

B. Displaced Morse oscillator model

To see the effects of a potential anharmonicity on the wave packet shaping, we adopt a displaced Morse oscillator model. For convenience, we introduce a unit energy $\hbar\omega$ to represent the model by a dimensionless coordinate. Here, we choose a harmonic frequency, ω, which is defined by

$$\omega=\tilde{\alpha}\sqrt{\frac{2\tilde{D}_e}{m}}, \tag{4.9}$$

where m is a mass, $\tilde{\alpha}$ is a range parameter, and $\tilde{D}_e$ is dissociation energy. Then the nuclear Hamiltonians in the electronically ground and excited states are, respectively, given by

$$h_g=\tfrac{1}{2}p^2+D_e\{[1-e^{-\alpha q}]^2-1\} \tag{4.10a}$$

and

$$h_e=\tfrac{1}{2}p^2+D_e\{[1-e^{-\alpha(q-\delta)}]^2-1\}, \tag{4.10b}$$

where the potential displacement is set to $\delta=3$. Here α and D_e are the dimensionless range parameter and dissociation

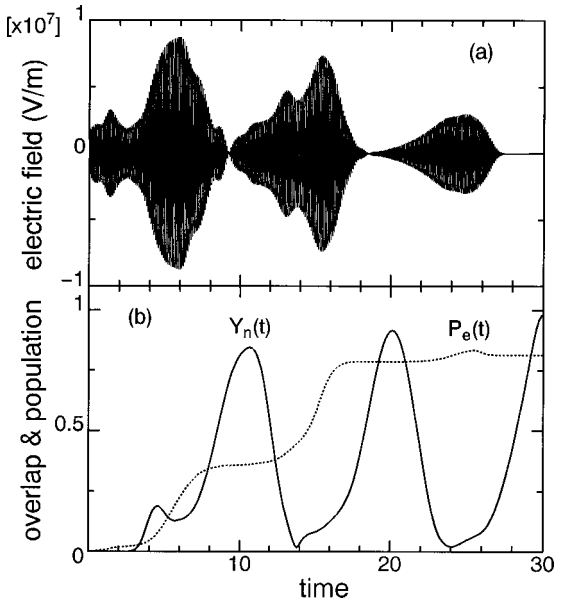

FIG. 14. Wave packet shaping for the target Gaussian with $(q_0,\sigma)=(12,0.5)$ in the case of a displaced Morse oscillator model. (a) Control pulse as a function of time, and (b) time-evolution of normalized overlap integral $Y_n(t)$ (solid line) and that of the excited population $P_e(t)$ (dotted line).

energy, respectively. Because of our special choice of the unit energy, these two parameters are related by

$$\alpha\sqrt{2D_e}=1. \tag{4.11}$$

In this example, the target Gaussian is located at the central position of $q_0=12$ and has a distribution width $\sigma=0.5$. It should be noted that this target Gaussian is confined in the well. We adopt the same target operator W with the same weight factors as those used in Sec. IV A. The amplitude parameter is set to $A=1.0\times10^9$. A calculated control pulse is shown in Fig. 14(a). This pulse has three pulse sequences corresponding to the period of the wave packet motion. Figure 14(b) shows the time evolution of the normalized overlap $Y_n(t)$ (solid line) and that of the excited population $P_e(t)$ (dotted line). From a large value of $Y_n(t_f)=0.98$, we can see that almost perfect shaping is realized for the excited population at a control time $t_f=30$, although $P_e(t_f)=0.81$.

The time- and frequency-resolved spectrum of the control pulse is shown in Fig. 15. All pulse sequences are down-chirped pulses. This is essential for the shaping of the bound wave packet in an anharmonic system such as a Morse oscillator model.[14,15] The period of wave packet motion depends on the vibrational energy due to the anharmonicity. For bound states, a superposition state of higher vibrational states has a longer period of motion. Therefore, wave packet components with a low velocity are first created by the high-frequency part of each pulse sequence. Then the high-velocity components are prepared around the Franck–Condon region by the low-frequency part of the control pulse. The high-velocity components of the wave packet catch up with the low-velocity components at the target position. They constructively interfere with each other so as to have a large overlap with the target Gaussian. To confirm

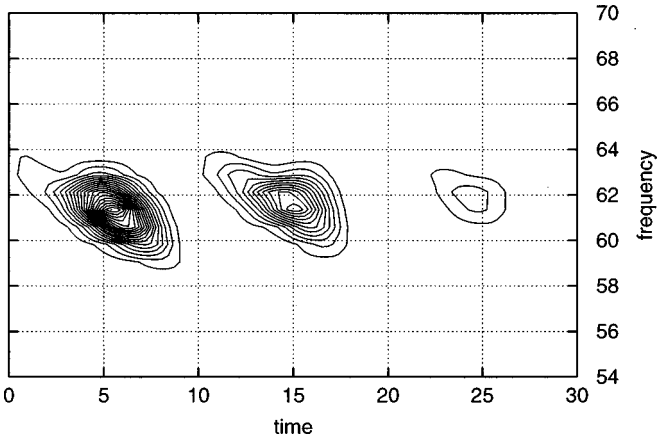

FIG. 15. Contour map of the time- and frequency-resolved spectrum of the control pulse in Fig. 14(a).

this wave packet-shaping mechanism, we also calculated the wave packet motion on the excited PES. Figure 16 shows snap shots of the wave packet motion for the last half period. The above mentioned shaping mechanism is the same as that found by Wilson's group in a weak-field regime based on the global control method.[14,15] This implies that the local control method can predict the same kinds of control pulse as that obtained by the optimal control method. Thus, the local control method can be a convenient alternative for wave packet shaping.

V. SUMMARY

We have proposed a novel local control method, starting with the optimal control theory. Our method requires a known function $g(t)$ *a priori*, which determines the path in the functional space of the objective functional. Thus, we

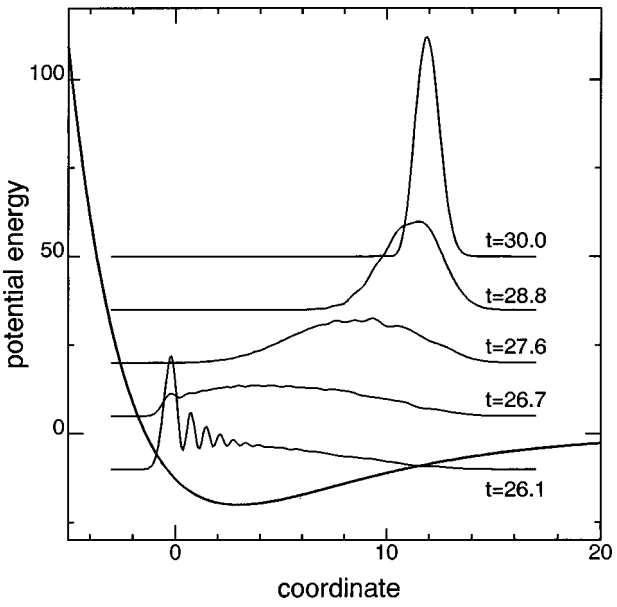

FIG. 16. Snap shots of the probability density $|\langle q|\phi_e(t)\rangle|^2$ for the last half period with an excited Morse potential.

have explicitly shown the relation between the local and optimal control methods. Here we would like to emphasize again that this function $g(t)$ is a given function of time and *should not* be a functional of electric fields. Our method also indicates the similarity between the local control method and the tracking problem, which is inverse quantum-mechanical control. In the special case of $g(t)=0$, our method gives the local control pulse derived by Kosloff *et al.*[3] by physical intuition.

Numerical examples were limited to the special case of $g(t)=0$. In order to see how the local control method designs control pulses, we applied this method to population control of few-level systems. The feedback mechanism of the local control pulse is analytically shown using a two-level system. For multilevel systems, the local control pulse includes several frequency components that correspond to transition energies. If modulation due to frequency mismatch appears before the control is completed, the control pulse consists of pulse sequences. On the other hand, if the control finishes earlier than this, then the control pulse is partially modulated and becomes a chirped pulse.

Combining an appropriate choice of target operator and the backward time-propagation technique allows us to apply the local control method to wave packet shaping. As an illustrative example, we adopted a two-electronic-surface model with displaced harmonic potentials and that with displaced Morse potentials. We chose a Gaussian function on the excited electronic PES as a target state whose probability density has a narrower width than the initial state $|g0\rangle$. The control pulse is composed of pulse sequences which have definite phase relation to efficiently excite the ground-state population using constructive interference. In the harmonic model, we discussed the structure of the control pulse, related to the distribution of the vibrational states included in the target Gaussian and that of the Franck–Condon factor. When there exists a large discrepancy between these distributions, the control pulse utilizes another interference mechanism to squeeze the wave packet. That is, the control pulse creates advanced and delayed components in the wave packet. The delayed component meets the advanced component which is reflected at the turning point. These components are designed so that they constructively interfere to create a large overlap with the target Gaussian at a control time. To realize such interference, the control pulse considerably changes its shape according to the forms of target Gaussians. In some cases, each pulse sequence of the control pulse consists of smaller pulse trains (Figs. 12 and 13), and may even become a chirped pulse (Figs. 8 and 9).

In the Morse oscillator model, the control pulse has a down-chirped structure since the target Gaussian has a zero average velocity and is confined in the well. The wave packet-shaping mechanism is essentially the same as that predicted by optimal control calculation in a weak-field regime by Wilson's group.[14,15] This implies that our local control scheme may be a convenient alternative to the global control methods in wave packet-shaping problems.

Finally we would like to comment on a choice of the function $g(t)$, although numerical examples presented in this paper are limited to the special case of $g(t)=0$. From Eq. (2.3), we can regard the function $g(t)$ as a path in the functional space, which represents the track for the time derivative of $F[\langle W(t)\rangle]$ and that for the penalty on the pulse energy. The former track may be determined by the same procedure as that in the inverse quantum-mechanical control developed by Rabitz's group.[30–32] An interesting point of our method is that we can also choose the track for the penalty on the pulse energy. For example, if we introduce an oscillating structure to the function $g(t)$, then the control pulse will include frequency components that reflect this oscillation. This implies that an appropriate choice of $g(t)$ may change the frequencies of the control pulse, and may make it possible to find another kind of control path which utilizes nonresonant optical transitions.

ACKNOWLEDGMENTS

We thank Professor H. Rabitz, Professor D. J. Tannor, Dr. W. Zhu, and Professor A. D. Bandrauk for their constructive comments and discussions. This work was partly supported by Development of High-Density Optical Pulse Generation and Advanced Material Control Techniques, Monbusho International Scientific Research Program (10044054) and Grants-in-Aid for Scientific Research, Nos. 09740511 and 90004473.

[1] A. P. Peirce, M. A. Dahleh, and H. Rabitz, Phys. Rev. A **37**, 4950 (1988).
[2] S. Shi and H. Rabitz, J. Chem. Phys. **92**, 364 (1990).
[3] R. Kosloff, S. A. Rice, P. Gaspard, S. Tersigni, and D. J. Tannor, Chem. Phys. **139**, 201 (1989).
[4] J. E. Combariza, B. Just, J. Manz, and G. K. Paramonov, J. Phys. Chem. **95**, 10351 (1991).
[5] D. J. Tannor, V. Kazakov, and V. Orlov, in *Time-Dependent Quantum Molecular Dynamics*, edited by J. Broeckhove and L. Lathouwers (Plenum, New York, 1992).
[6] J. Somlói, V. A. Kazakov, and D. J. Tannor, Chem. Phys. **172**, 85 (1993).
[7] H. Shen, J.-P. Dussault, and A. D. Bandrauk, Chem. Phys. Lett. **221**, 498 (1994).
[8] W. Zhu, J. Botina, and H. Rabitz, J. Chem. Phys. **108**, 1953 (1998).
[9] W. Zhu and H. Rabitz, J. Chem. Phys. **109**, 385 (1998).
[10] D. J. Tannor and S. A. Rice, J. Chem. Phys. **83**, 5013 (1985).
[11] I. Averbukh and M. Shapiro, Phys. Rev. A **47**, 5086 (1993).
[12] D. G. Abrashkevich, I. S. Averbukh, and M. Shapiro, J. Chem. Phys. **101**, 9295 (1994).
[13] Y. Yan, R. E. Gillilan, R. M. Whitnell, K. R. Wilson, and S. Mukamel, J. Phys. Chem. **97**, 2320 (1993).
[14] J. L. Krause, R. M. Whitnell, K. R. Wilson, Y. Yan, and S. Mukamel, J. Chem. Phys. **99**, 6562 (1993).
[15] B. Kohler, V. V. Yakovlev, J. Che, J. L. Krause, M. Messina, K. R. Wilson, N. Schwentner, R. M. Whitnell, and Y. Yan, Phys. Rev. Lett. **74**, 3360 (1995).
[16] Y. Yan, J. Cao, and Z. Shen, J. Chem. Phys. **107**, 3471 (1997).
[17] L. Shen, S. Shi, and H. Rabitz, J. Phys. Chem. **97**, 8874 (1993).
[18] L. Shen, S. Shi, and H. Rabitz, J. Phys. Chem. **97**, 12114 (1993).
[19] V. Dubov and H. Rabitz, Chem. Phys. Lett. **235**, 309 (1995).
[20] V. Dubov and H. Rabitz, J. Chem. Phys. **103**, 8412 (1995).
[21] R. Kosloff, A. D. Hammerich, and D. J. Tannor, Phys. Rev. Lett. **69**, 2172 (1992).
[22] A. Bartana, R. Kosloff, and D. J. Tannor, J. Chem. Phys. **99**, 196 (1993).
[23] D. J. Tannor, in *Molecules in Laser Fields*, edited by A. D. Bandrauk (Dekker, New York, 1994).
[24] A. Bartana, R. Kosloff, and D. J. Tannor, J. Chem. Phys. **106**, 1435 (1997).
[25] V. Malinovsky, C. Meier, and D. J. Tannor, Chem. Phys. **221**, 67 (1997).
[26] V. S. Malinovsky and D. J. Tannor, Phys. Rev. A **56**, 4929 (1997).

[27] H. Tang, R. Kosloff, and S. A. Rice, J. Chem. Phys. **104**, 5457 (1996).
[28] M. Sugawara and Y. Fujimura, J. Chem. Phys. **100**, 5646 (1994).
[29] Y. Ohtsuki, Y. Yahata, H. Kono, and Y. Fujimura, Chem. Phys. Lett. **287**, 627 (1998).
[30] P. Gross, H. Singh, H. Rabitz, K. Mease, and G. M. Huang, Phys. Rev. A **47**, 4593 (1993).
[31] G. M. Huang, P. Gross, H. Singh, H. Rabitz, and K. Mease, IEEE Conf. No. 32 **2**, 1930 (1993).
[32] Y. Chen, P. Gross, V. Ramakrishna, and H. Rabitz, J. Chem. Phys. **102**, 8001 (1995).
[33] T. T. Nguyen-Dang, C. Chatelas, and D. Tanguay, J. Chem. Phys. **102**, 1528 (1995).
[34] S. Chelkowski, A. D. Bandrauk, and P. B. Corkum, Phys. Rev. Lett. **65**, 2355 (1990).
[35] S. Chelkowski and A. D. Bandrauk, Chem. Phys. Lett. **186**, 264 (1991).